Supporting Information for:

Unsaturated Chiral-only-at-Metal Rhodium(III) Complexes bearing SiN-type Ligands

Unai Prieto-Pascual,[a] Itxaso Bustos,[a] Pablo Salcedo-Abraira,[b] Iñigo J. Vitorica-Yrezabal,[b] Aitor Landa,[a] Zoraida Freixa,*[ac] and Miguel A. Huertos*[ac]

a) Department of Applied Chemistry, University of Basque Country (UPV/EHU), 20080 San Sebastián, SPAIN.
b) Department of Inorganic Chemistry, University of Granada, 18071, Granada, SPAIN
c) IKERBASQUE. Basque Foundation for Science, 48013, Bilbao, SPAIN.

1. General Considerations

All manipulations, unless otherwise stated, were performed under an atmosphere of argon, using standard Schlenk techniques. Glassware was oven-dried at 110 ºC overnight and flamed under vacuum prior to use. Dry and oxygen-free solvents were employed. *rac*-**Rh(SiN)$_2$Cl**,[1] 8-(dimethylsilyl)quinoline,[2] Na[S-B(R-Man)$_2$],[3] Na[R-B(S-Man)$_2$][3] and Na[BAr$^F{}_4$][4] were prepared as previously described. NMR spectra were recorded on Bruker Ultra Shift 500 MHz and Bruker Advance DPX 300 MHz spectrometer. ^{1}H and ^{13}C NMR spectra were referenced to the residual solvent signals and ^{29}Si NMR spectra were referenced against Me_4Si (TMS). Chemical shifts are quoted in ppm and coupling constants in Hz. ESI-MS was recorded on LC-Q-TOF with Agilent Jet Stream ESI ionization source. The topographic maps were constructed using ionic fragments extracted from the corresponding X-ray structures of L-Rh(SiN)(S-B(R-Man)$_2$) and D-Rh(SiN)(R-B(S-Man)$_2$) using SambVca 2.1.[5] The rhodium and the boron atoms, respectively, have been defined as the origin of coordinates, with the counterpart (boron and rhodium, respectively) defining the positive z axis. To calculate the topographic maps, a sphere of radius 3.5 Å is centered at z= 0 Å was constructed. Bond radii were scaled by 1.17, as suggested for related calculations. Hydrogen atoms have been included in the calculation. The most important considerations about X-ray, ECD and catalytic experiments will be discussed below in the specific sub-sections of this supporting information.

2. Synthesis and characterization of *rac*-Rh(SiN)$_2$Cl

Compound *rac*-**Rh(SiN)$_2$Cl** was prepared as described in reference 1. However, the characterization of *rac*-**Rh(SiN)$_2$Cl** has been depicted for a clearer description of the work.

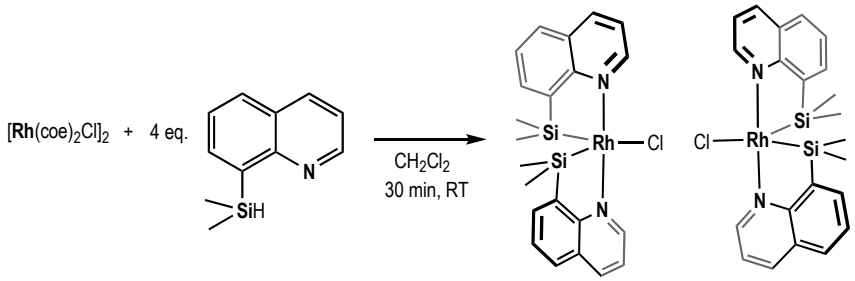

Scheme 1. Synthesis of complex *rac*-**Rh(SiN)$_2$Cl**

^{1}H RMN (500 MHz, $CDCl_3$): δ 9.82 (dt, $J_{1(H-H)}$ = 5.2 Hz, $J_{2(H-H)}$ = 1.4 Hz, 2H$_{arom.}$), 8.24 (dd, $J_{1(H-H)}$ = 8.2 Hz, $J_{2(H-H)}$ = 1.4 Hz, 2H$_{arom.}$), 7.86 (dd, $J_{1(H-H)}$ = 6.7 Hz, $J_{2(H-H)}$ = 1.4 Hz, 2H$_{arom.}$), 7.79 (dd, $J_{1(H-H)}$ = 8.2 Hz, $J_{2(H-H)}$ = 1.4 Hz, 2H$_{arom.}$), 7.57 (dd, $J_{1(H-H)}$ = 8.2 Hz, $J_{2(H-H)}$ = 6.7 Hz, 2H$_{arom.}$), 7.42 (dd, $J_{1(H-H)}$ = 8.2 Hz, $J_{2(H-H)}$ = 5.2 Hz, 2H$_{arom.}$), 0.57 (s, 6H, Si-CH_3), -0.22 (s, 6H, Si-CH_3).
^{13}C{^{1}H} RMN (125 MHz, $CDCl_3$): δ 158-122 (18C$_{arom.}$), 6.9 (2C, Si-CH_3), 0.4 (2C, Si-CH_3).

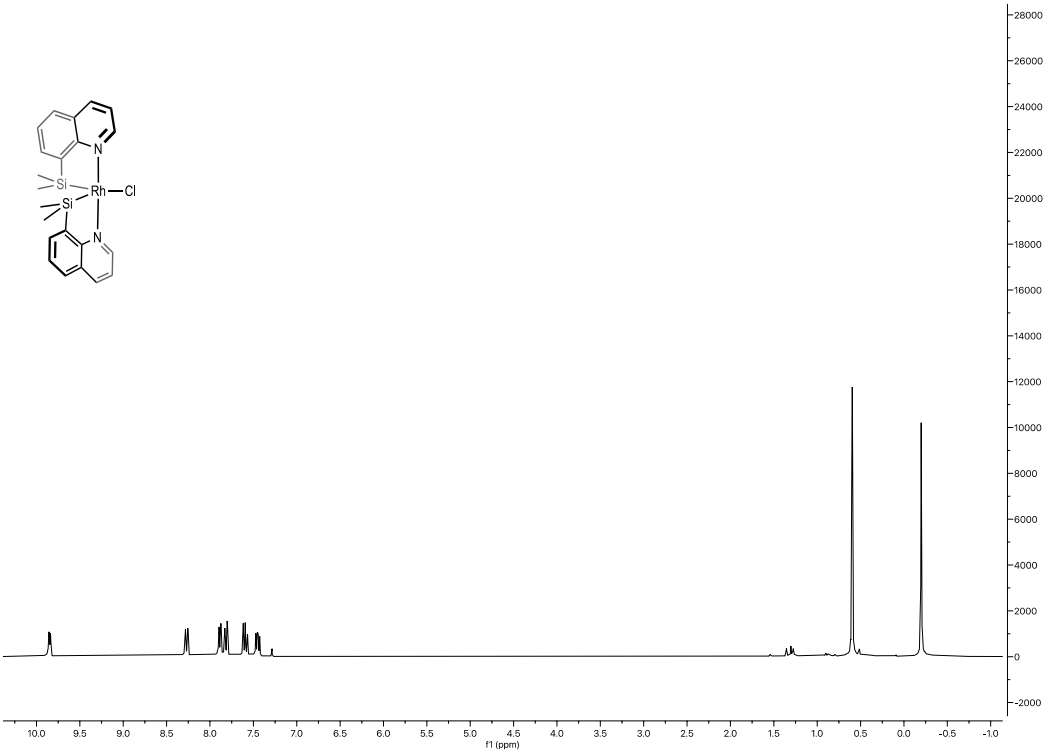

Figure S.1. ^{1}H NMR ($CDCl_3$) of *rac*-**Rh(SiN)$_2$Cl.**

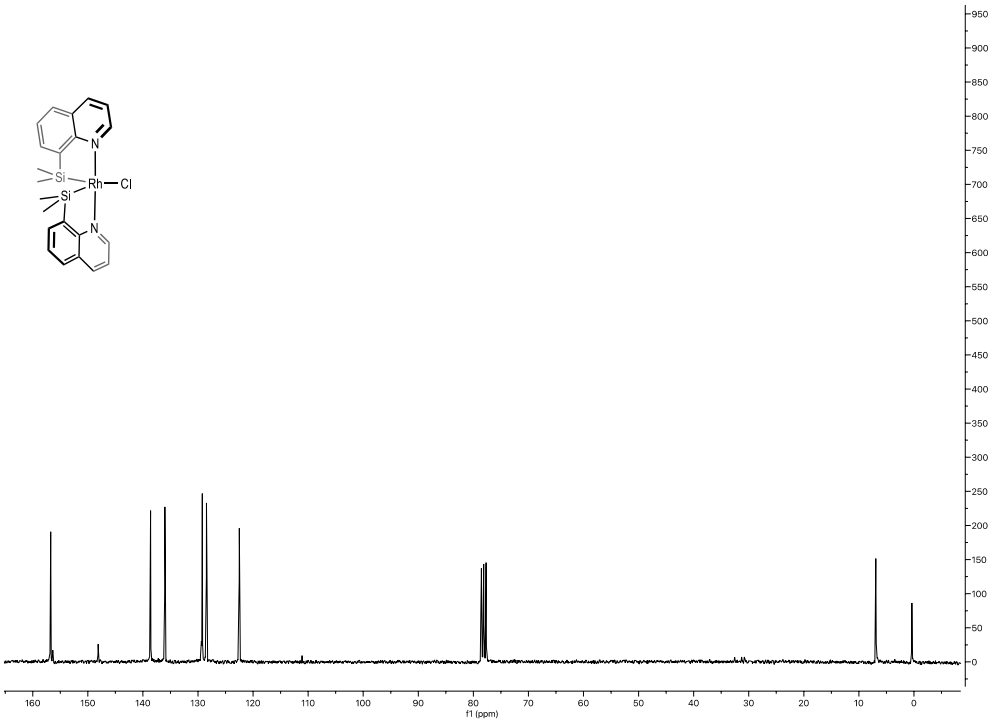

Figure S.2. $^{13}C\{^{1}H\}$ NMR ($CDCl_3$) of *rac*-**Rh(SiN)$_2$Cl.**

3. Resolution of *rac*-Rh(SiN)$_2$Cl. Synthesis and characterization of Δ-Rh(SiN)$_2$(*R*-B(*S*-Man)$_2$), Λ-Rh(SiN)$_2$(*S*-B(*R*-Man)$_2$), Δ-Rh(SiN)$_2$Cl, Λ-Rh(SiN)$_2$Cl, Δ-Rh(SiN)$_2$[BAr$^F_4$] and Λ-Rh(SiN)$_2$[BAr$^F_4$].

Scheme S2 shows a reaction diagram for the synthesis of complexes **Δ-Rh(SiN)$_2$(*R*-B(*S*-Man)$_2$), Λ-Rh(SiN)$_2$(*S*-B(*R*-Man)$_2$), Δ-Rh(SiN)$_2$Cl, Λ-Rh(SiN)$_2$Cl, Δ-Rh(SiN)$_2$[BAr$^F_4$] and Λ-Rh(SiN)$_2$[BAr$^F_4$].**

Procedure:

The reaction of ***rac*-Rh(SiN)$_2$Cl** (100 mg, 0.19 mmol) with the chiral auxiliary Na[S-B(R-Man)$_2$] (65 mg, 0.19 mmol) in CH_2Cl_2/MeOH (6 mL/2 mL) at room temperature for 30 min of reaction. This mixture was dried, redissolved in CH_2Cl_2 and filtered to remove NaCl, and the residue (112 mg, 0.15 mmol, 78 % yield) was analyzed by ^{1}H NMR in $CDCl_3$ (Figure S.3). The residue was dissolved in CH_2Cl_2 and crystallized by slow diffusion of pentane. Enantiopure **Λ-Rh(SiN)$_2$[S-B(R-Man)$_2$]** (48 mg, 0.06 mmol) was obtained as the crystalline solid that precipitated (34 % yield).

After separation of **Λ-Rh(SiN)$_2$[S-B(R-Man)$_2$]** by filtration, the solvent of the mother liquor was removed under vacuum and the residue was dissolved in CH_2Cl_2 (2 mL) and washed with brine (2 mL) at room temperature for 30 minutes. After the separation of the organic phase, it was dried over $MgSO_4$, and the solvent was evaporated under reduced pressure to obtain a Δ-enriched mixture of Δ/Λ-**Rh(SiN)$_2$Cl** isomers (55 mg, 0.11 mmol). This mixture was reacted with Na[R-B(S-Man)$_2$] (37 mg, 0.11 mmol) in CH_2Cl_2/MeOH (6 mL/2 mL) at room temperature for 30 min. After evaporation of the solvent, crystallization by diffusion of pentane on a CH_2Cl_2 solution of this mixture gave crystals of the enantiopure complex **Δ-Rh(SiN)$_2$(R-B(S-Man)$_2$)** (39 mg, 0,05 mmol, 27% yield).

Independently, enantiopure complexes **Λ-Rh(SiN)$_2$(S-B(R-Man)$_2$)** and **Δ-Rh(SiN)$_2$(R-B(S-Man)$_2$)** (50 mg, 0.07 mmol) were dissolved in CH_2Cl_2 (2 mL) and washed with brine (2 mL) at room temperature for 30 minutes. After the separation of the organic phase, it was dried over $MgSO_4$, and the solvent was evaporated under reduced pressure to obtain **Λ-Rh(SiN)$_2$Cl** (32 mg, 0.06 mmol, 94% yield) and Δ-**Rh(SiN)$_2$Cl** (33 mg, 0.06 mmol, 95% yield) respectively.

In a Schlenk flask, enantiopure complexes **Λ-Rh(SiN)$_2$(S-B(R-Man)$_2$)** and **Δ-Rh(SiN)$_2$(R-B(S-Man)$_2$)** (50 mg, 0.07 mmol) were independently reacted with Na[BAr$^F_4$] (71 mg, 0.08 mmol) in CH_2Cl_2 (2 mL) under argon. After 30 minutes, the reaction mixture was filtered to remove the formed NaCl. After removing the solvent from the filtrate by evaporation, enantiopure cationic complexes **Λ-Rh(SiN)$_2$[BAr$^F_4$]** (75 mg, 0.05 mmol, 86% yield) and **Δ-Rh(SiN)$_2$[BAr$^F_4$]** (71 mg, 0.05 mmol, 78% yield) were obtained, respectively.

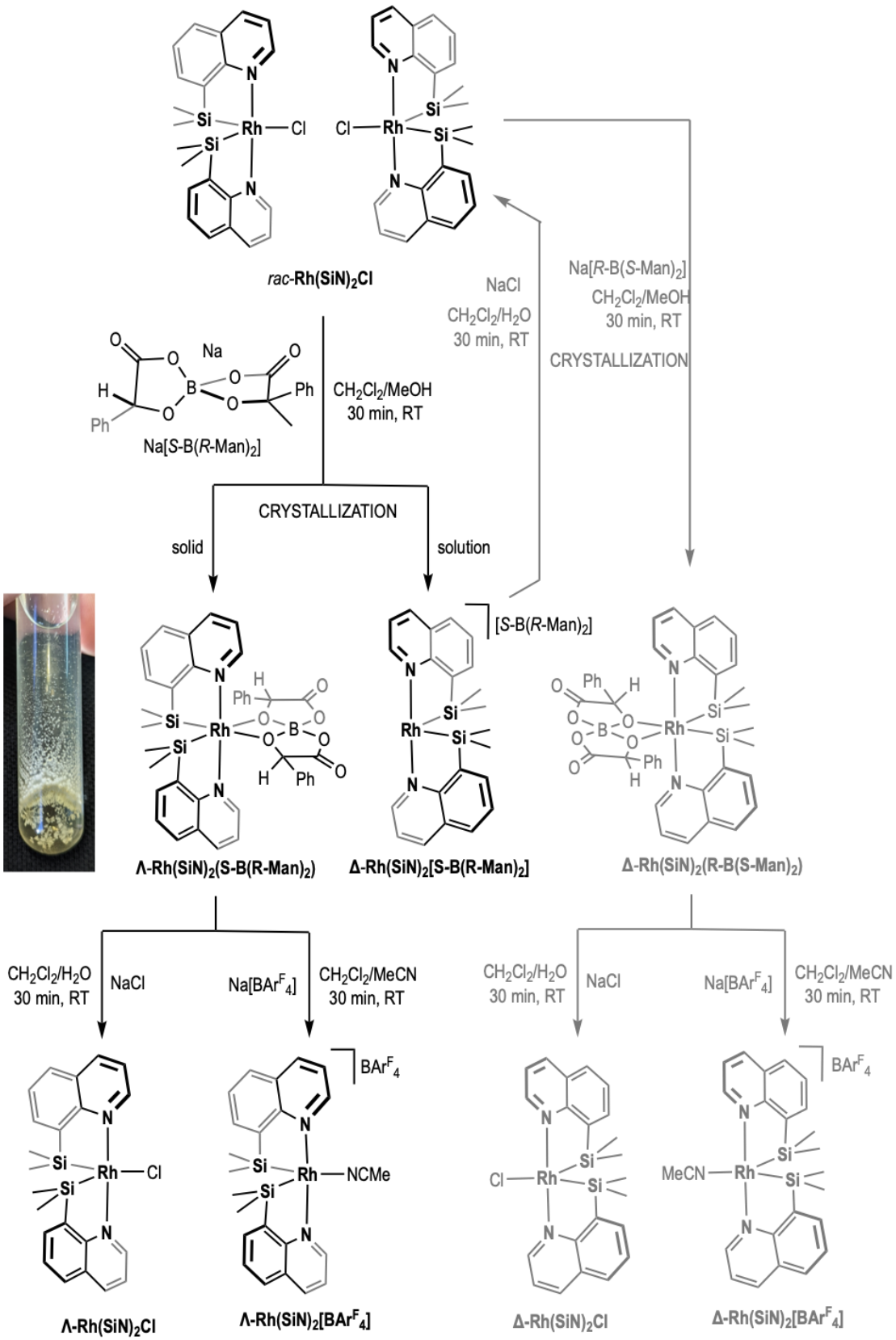

Scheme S.2. Spiroborate anions-mediated resolution of *rac*-**Rh(SiN)$_2$Cl**

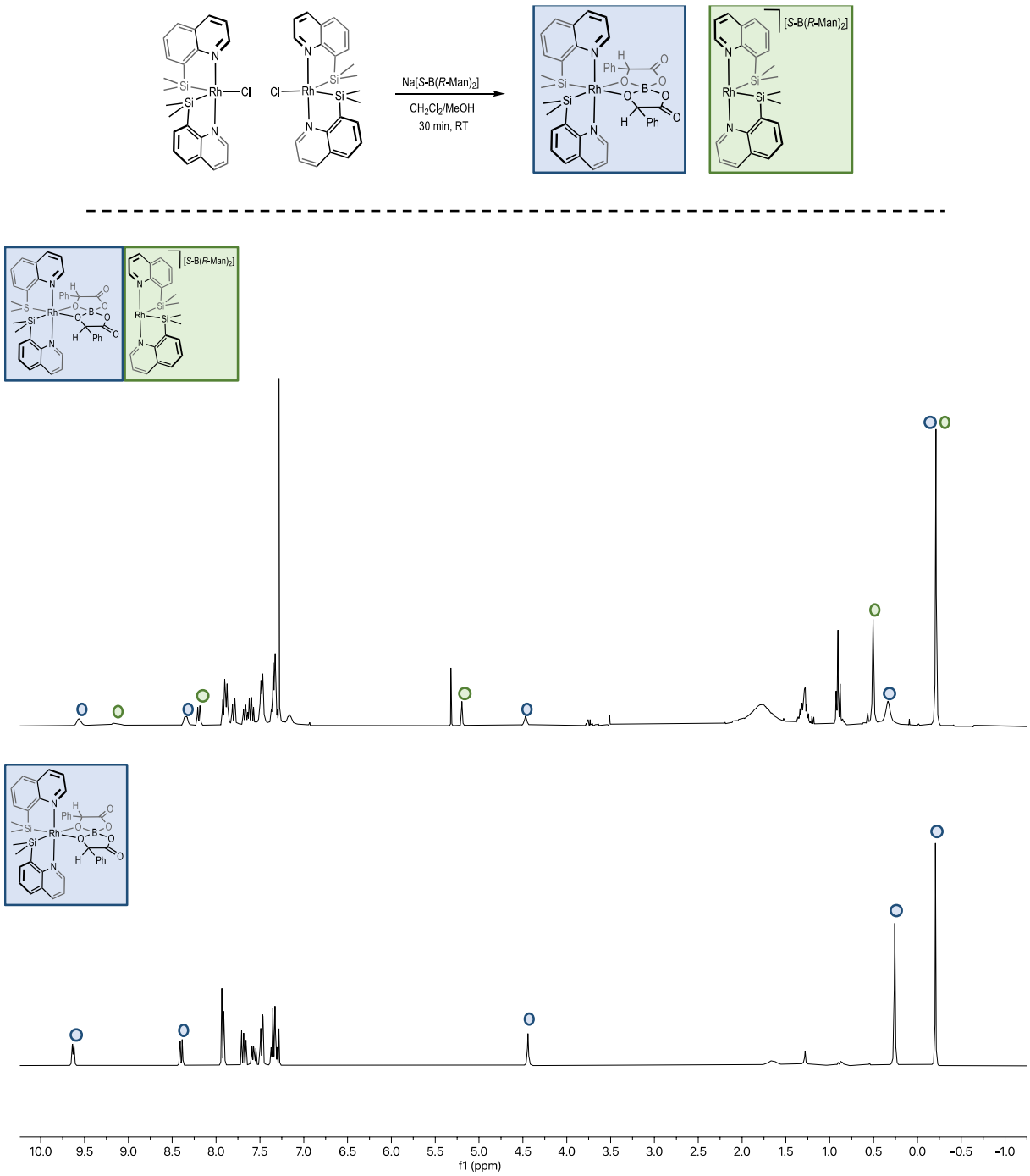

Figure S.3. ^{1}H NMR ($CDCl_3$) mixture of isomers after reaction of *rac*-**Rh(SiN)$_2$Cl** with Na[S-B(R-Man)$_2$] (top). ^{1}H NMR ($CDCl_3$) of isolated crystals of **Λ-Rh(SiN)$_2$(*S*-B(*R*-Man)$_2$)** (bottom).

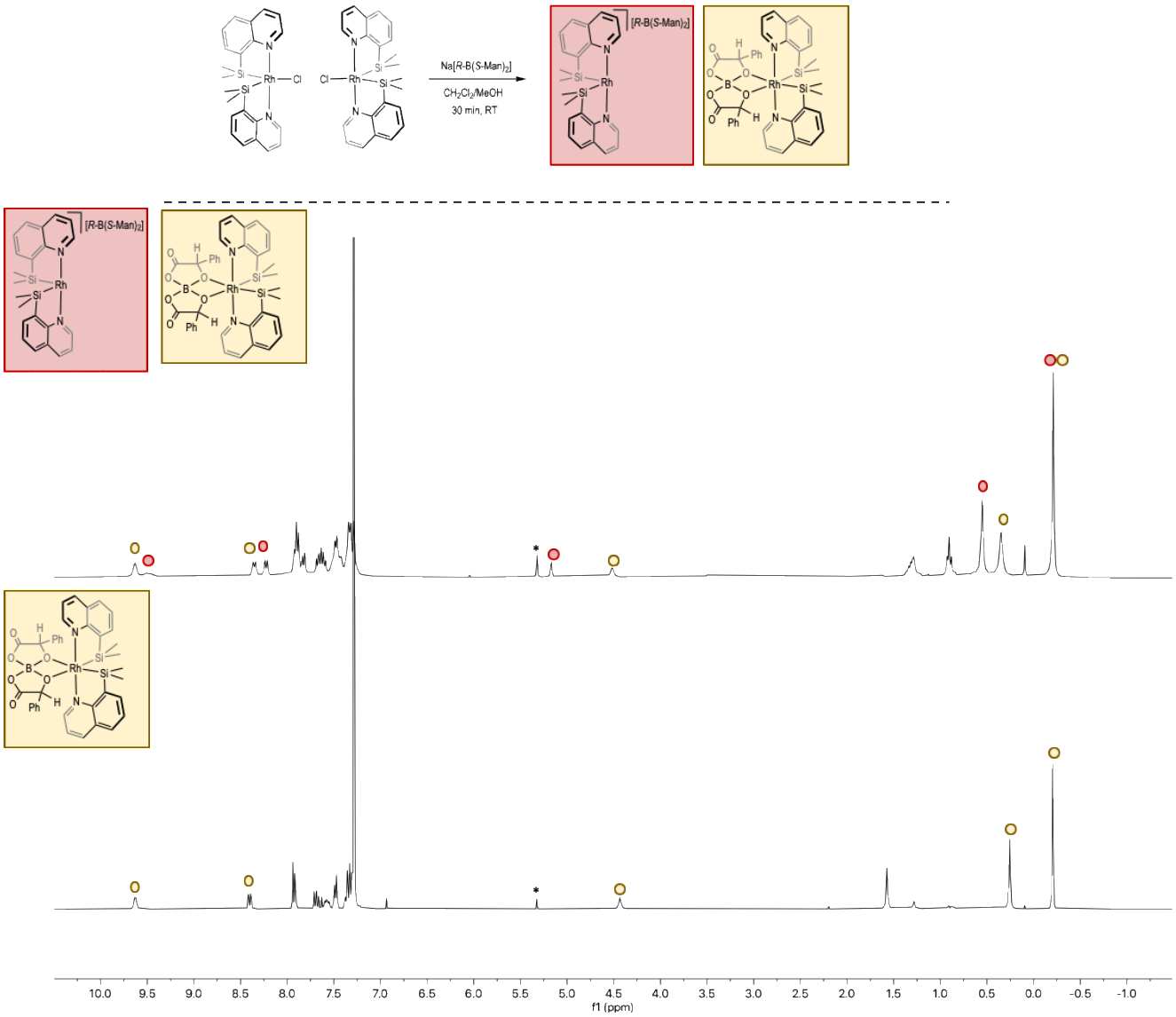

Figure S.4. ^{1}H NMR ($CDCl_3$) mixture of isomers after reaction of *rac*-**Rh(SiN)$_2$Cl** with Na[R-B(S-Man)$_2$] (top). ^{1}H NMR ($CDCl_3$) of isolated crystals of **Δ-Rh(SiN)$_2$(*R*-B(*S*-Man)$_2$)** (bottom). ✻= CH_2Cl_2.

· Characterization of Δ-Rh(SiN)$_2$(*R*-B(*S*-Man)$_2$), Λ-Rh(SiN)$_2$(*S*-B(*R*-Man)$_2$)

^{1}H NMR (300 MHz, $CDCl_3$): δ 9.61 (d, $J_{3(H-H)}$ = 5.7 Hz, 2H$_{arom.}$SiN), 8.38 (dd, $J_{3(H-H)}$ = 8.2 Hz, $J_{4(H-H)}$ = 1.3 Hz, 2H$_{arom.}$ SiN), 7.91 (m, 2H$_{arom.}$ Ph), 7.90 (m, 2H$_{arom.}$ SiN), 7.66 (dd, $J_{3(H-H)}$ = 8.1 Hz, $J_{3(H-H)}$ = 6.7 Hz, 2H$_{arom.}$ SiN), 7.54 (dd, $J_{3(H-H)}$ = 8.5 Hz, $J_{2(H-H)}$ = 5.4 Hz, 2H$_{arom.}$ SiN), 7.46 (m, 2H$_{arom.}$ Ph), 7.45 (m, 2H$_{arom.}$ SiN), 7.36-7.27 (6H$_{arom.}$ Ph), 4.42 (s, 2H mandelate) 0.24 (s, 6H, Si-CH_3), -0.23 (s, 6H, Si-CH_3).

^{13}C{^{1}H} NMR (75 MHz, $CDCl_3$): δ 176.5 (2C, C=O), 156.2 (2C$_{arom.}$), 154.3 (2C$_{arom.}$), 147.6 (2C$_{arom.}$), 139.9 (2C$_{arom.}$), 138.7 (2C$_{arom.}$), 136.8 (2C$_{arom.}$), 129.9 (2C$_{arom.}$), 129.7 (4C$_{arom.}$), 129.4 (2C$_{arom.}$), 129.1 (2C$_{arom.}$), 127.4 (4C$_{arom.}$), 123.1 (2C$_{arom.}$), 111,1 (2C$_{arom.}$), 80.2 (2C, mandelate) 5.2 (2C, Si-CH_3), 0.8 (2C, Si-CH_3).

^{11}B{^{1}H} NMR (160 MHz, $CDCl_3$): δ 12.2

^{29}Si NMR (Chemical sift from ^{1}H-^{29}Si HMBC) (500 MHz, $CDCl_3$): δ 47.1

ESI-MS (MeCN): calc: 475.054; found m/z 475.053. For the ion $[C_{22}H_{24}N_2RhSi_2]^+$.

· Characterization of Δ-Rh(SiN)$_2$Cl and Λ-Rh(SiN)$_2$Cl

^{1}H NMR (300 MHz, $CDCl_3$): δ 9.82 (d, $J_{3(H-H)}$ = 5.2 Hz, 2H$_{arom.}$), 8.25 (d, $J_{3(H-H)}$ = 8.2 Hz, 2H$_{arom.}$), 7.86 (d, $J_{3(H-H)}$ = 6.7 Hz, 2H$_{arom.}$), 7.79 (d, $J_{3(H-H)}$ = 8.2 Hz, 2H$_{arom.}$), 7.57 (t, $J_{3(H-H)}$ = 8.2 Hz, 2H$_{arom.}$), 7.43 (dd, $J_{1(H-H)}$ = 8.2 Hz, $J_{2(H-H)}$ = 5.2 Hz, 2H$_{arom.}$), 0.57 (s, 6H, Si-CH_3), -0.22 (s, 6H, Si-CH_3).

^{13}C{^{1}H} NMR (75 MHz, $CDCl_3$): δ 156.3 (2C$_{arom.}$), 155.9 (2C$_{arom.}$), 147.7 (2C$_{arom.}$), 138.2 (2C$_{arom.}$), 135.6 (2C$_{arom.}$), 129.0 (2C$_{arom.}$), 128.7 (2C$_{arom.}$), 128.1 (2C$_{arom.}$), 122.1 (2C$_{arom.}$), 6.5 (2C, Si-CH_3),-0.1 (2C, Si-CH_3).

^{29}Si NMR (Chemical sift from ^{1}H-^{29}Si HMBC) (500 MHz, $CDCl_3$): δ 48.8

ESI-MS (MeCN): calc: 475.054; found m/z 475.055. For the ion $[C_{22}H_{24}N_2RhSi_2]^+$.

· Characterization of Δ-Rh(SiN)$_2$[BAr$^F_4$] and Λ-Rh(SiN)$_2$[BAr$^F_4$]

^{1}H NMR (300 MHz, CD_2Cl_2): δ 9.10 (S$_{broad}$, 2H$_{arom.}$), 8.42 (S$_{broad}$, 2H$_{arom.}$), 7.95 (t$_{broad}$, $J_{3(H-H)}$ = 7.2 Hz,4H$_{arom.}$), 7.73 (s, 8H$_{arom.}$, BAr$^F_4$), 7.70 (m, 2H$_{arom.}$), 7.56 (s, 4H$_{arom.}$, BAr$^F_4$) 7.52 (S$_{broad}$, 2H$_{arom.}$), 2.26 (s, 3H, MeCN), 0.55 (s, 6H, Si-CH_3), -0.18 (s, 6H, Si-CH_3).

^{13}C{^{1}H} NMR (75 MHz, CD_2Cl_2): δ 162.0 (q, J_{B-C} = 50 Hz, BAr$^F_4$), 154.9 (2C$_{arom.}$), 153.3 (2C$_{arom.}$), 145.6 (2C$_{arom.}$), 139.7 (2C$_{arom.}$), 136.5 (2C$_{arom.}$), 135.0 (s, BAr$^F_4$), 129.2 (2C$_{arom.}$), 129.0 (q, J_{F-C} = 12 Hz, BAr$^F_4$), 128.6(2C$_{arom.}$), 124.7 (q, J_{F-C} = 273 Hz, CF_3), 121.8 (2C$_{arom.}$), 119.9(2C$_{arom.}$), 119.5 (s, 1C, CH_3CN), 117.6 (m, BAr$^F_4$), 4.9 (2C, Si-CH_3), 2.7 (1C, CH_3CN), -0.7 (2C, Si-CH_3).

^{29}Si NMR (Chemical sift from ^{1}H-^{29}Si HMBC) (500 MHz, CD_2Cl_2): δ 52.2

ESI-MS (MeCN): calc: 475.054; found m/z 475.054. For the ion $[C_{22}H_{24}N_2RhSi_2]^+$.

4. NMR spectra of complexes

4.1 Δ-Rh(SiN)$_2$(*R*-B(*S*-Man)$_2$), Λ-Rh(SiN)$_2$(*S*-B(*R*-Man)$_2$)

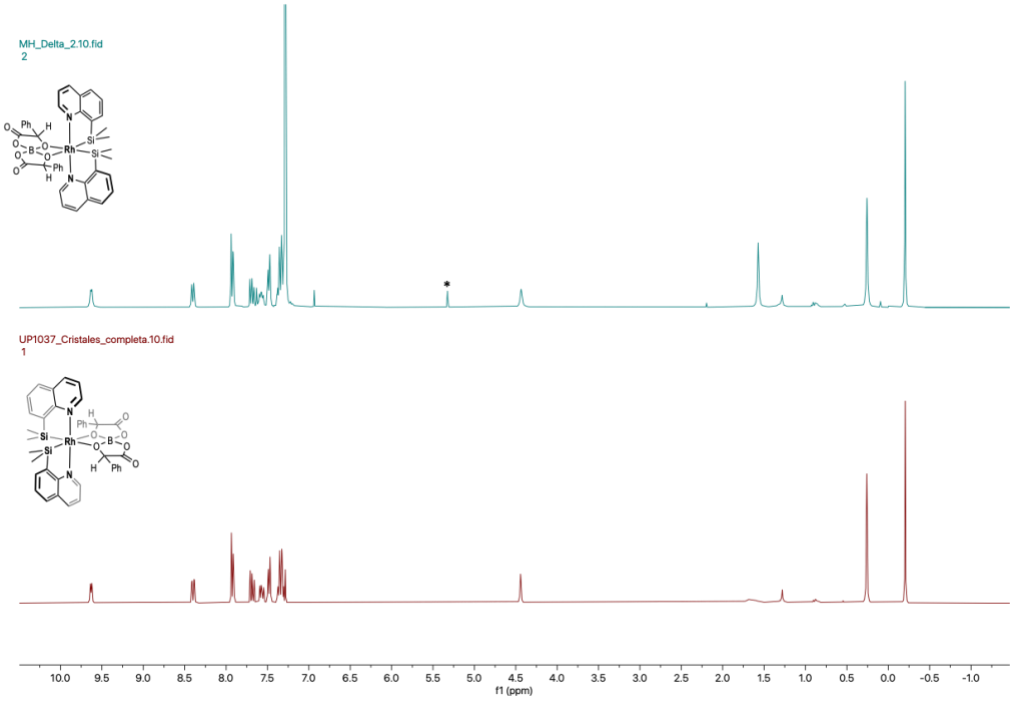

Figure S.5. ^{1}H NMR ($CDCl_3$) comparison between **Δ-Rh(SiN)$_2$(*R*-B(*S*-Man)$_2$), Λ-Rh(SiN)$_2$(*S*-B(*R*-Man)$_2$).** ✻= CH_2Cl_2.

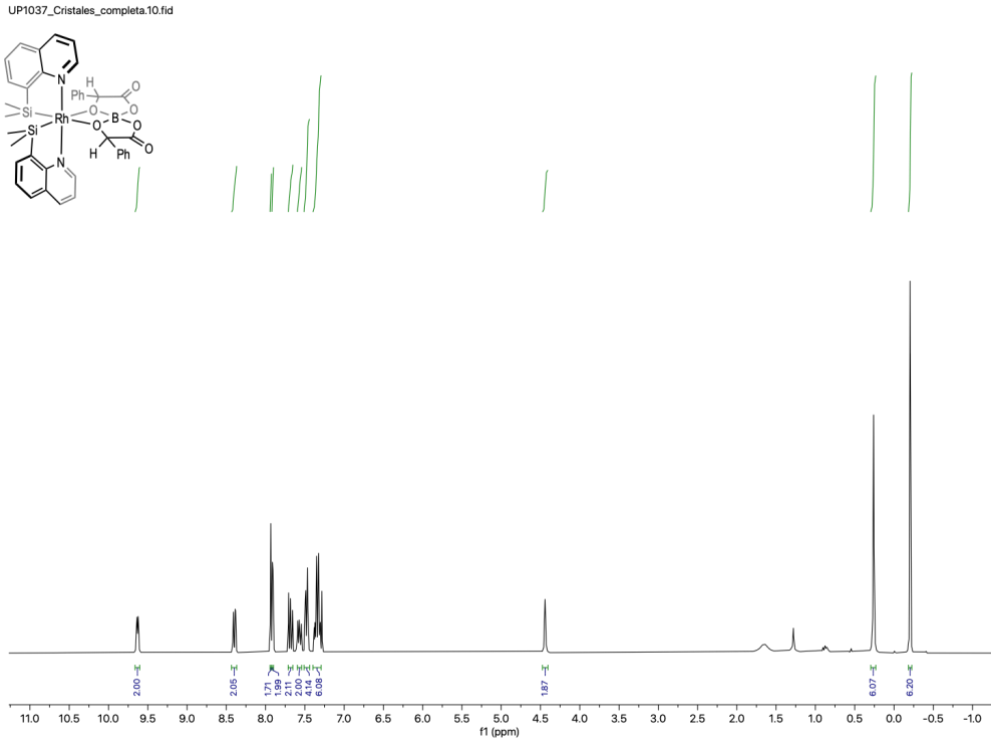

Figure S.6. ^{1}H NMR ($CDCl_3$) of **Λ-Rh(SiN)$_2$(*S*-B(*R*-Man)$_2$).**

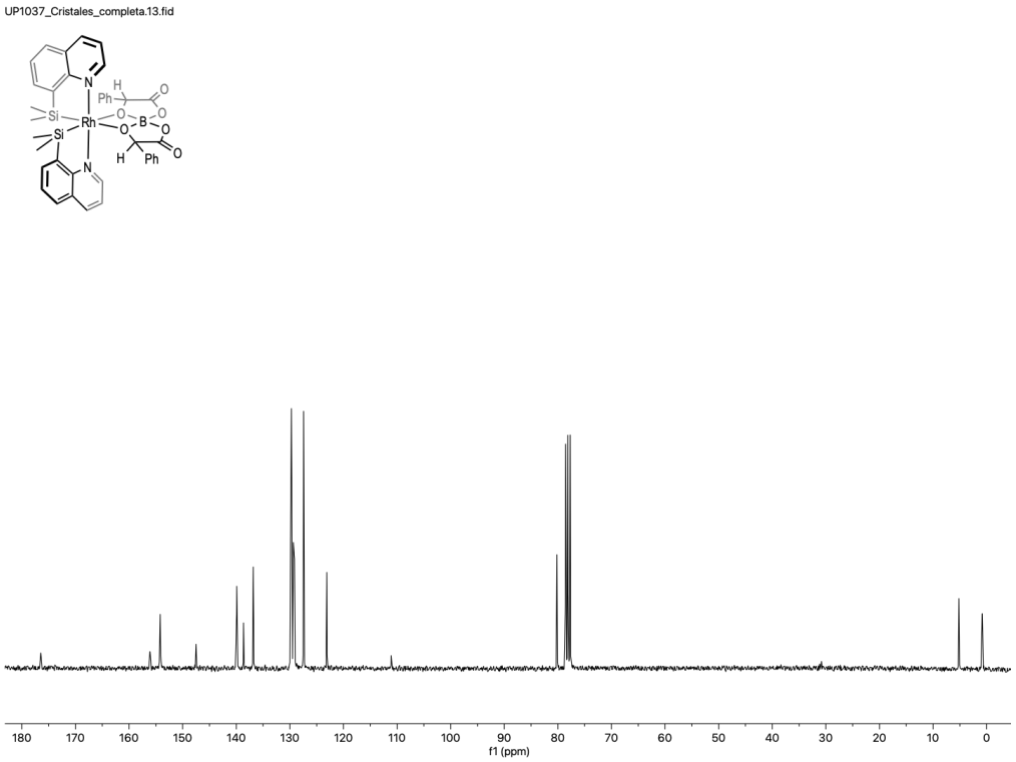

Figure S.7. $^{13}C\{^{1}H\}$ NMR ($CDCl_3$) of **Λ-Rh(SiN)$_2$(*S*-B(*R*-Man)$_2$)..**

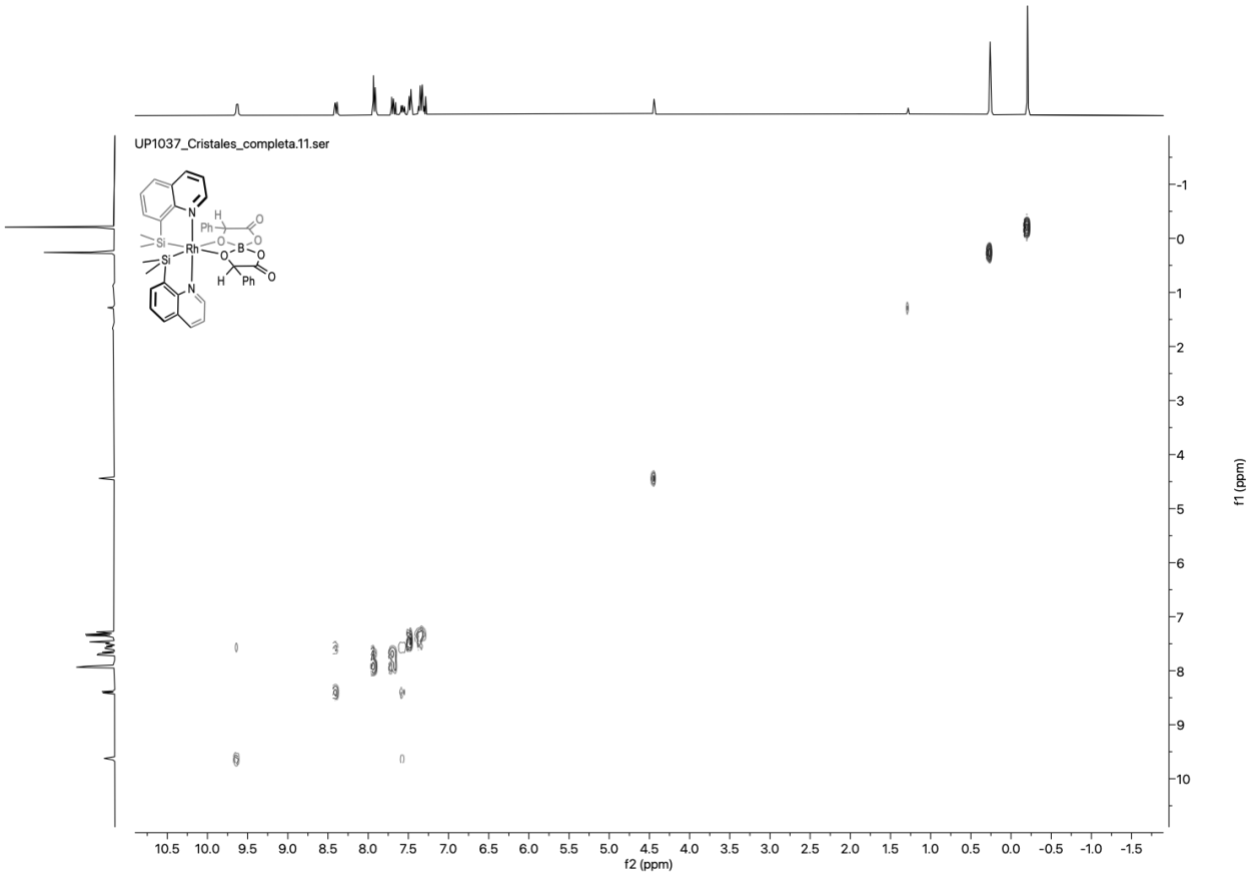

Figure S.8. $^{1}H/^{1}H$ COSY NMR ($CDCl_3$) of **Λ-Rh(SiN)$_2$(*S*-B(*R*-Man)$_2$).**

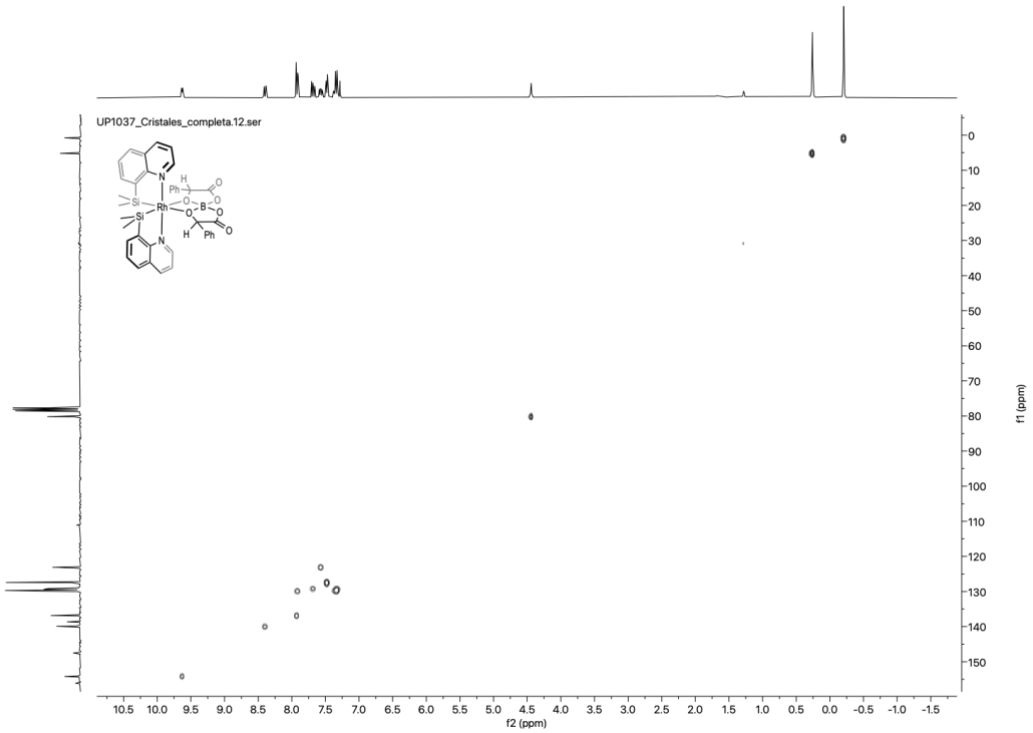

Figure S.9. $^{13}C/^{1}H$ HSQC NMR ($CDCl_3$) of **Λ-Rh(SiN)$_2$(*S*-B(*R*- Man)$_2$).**

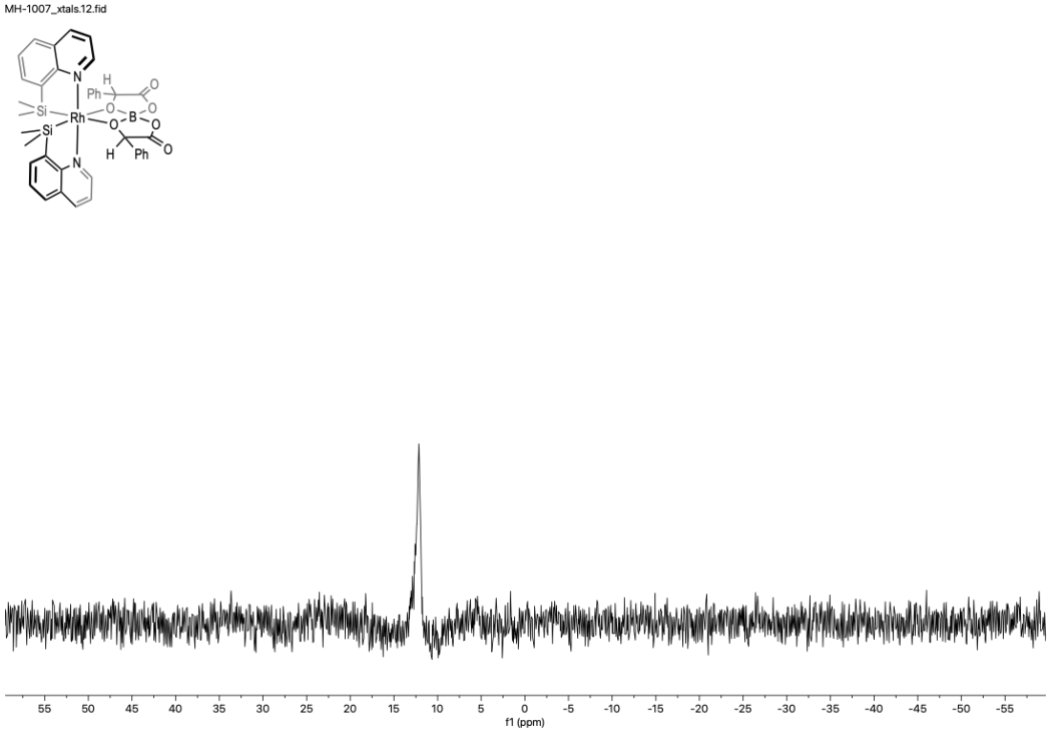

Figure S.10. $^{11}B\{^{1}H\}$ NMR ($CDCl_3$) of **Λ-Rh(SiN)$_2$(*S*-B(*R*-Man)$_2$).**

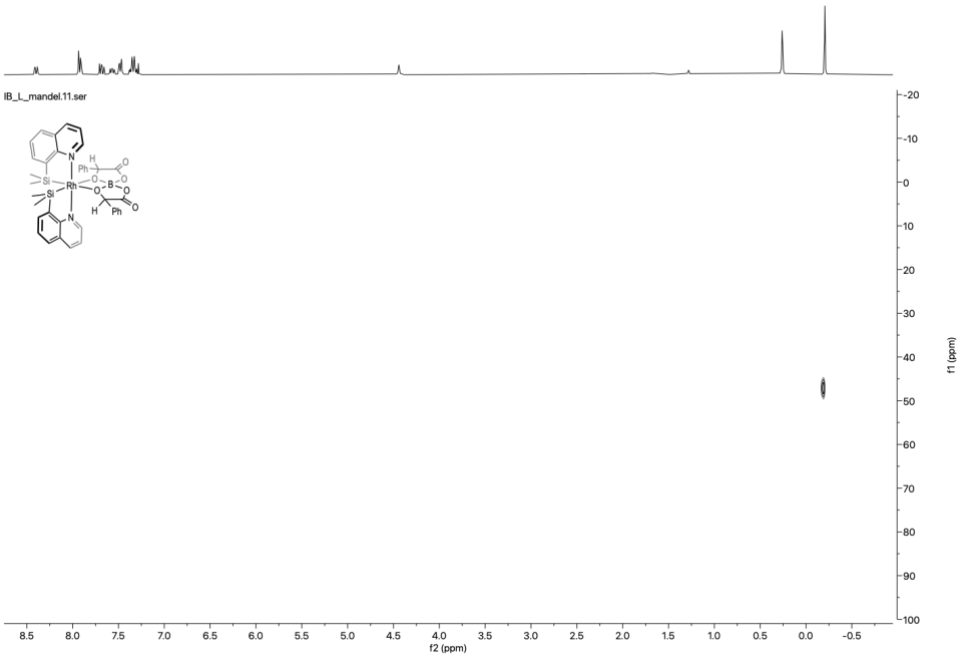

Figure S.11. $^{1}H/^{29}Si$ HMBC NMR ($CDCl_3$) of **Λ-Rh(SiN)$_2$(*S*-B(*R*-Man)$_2$).**

4.2 Δ-Rh(SiN)Cl and Λ-Rh(SiN)Cl.

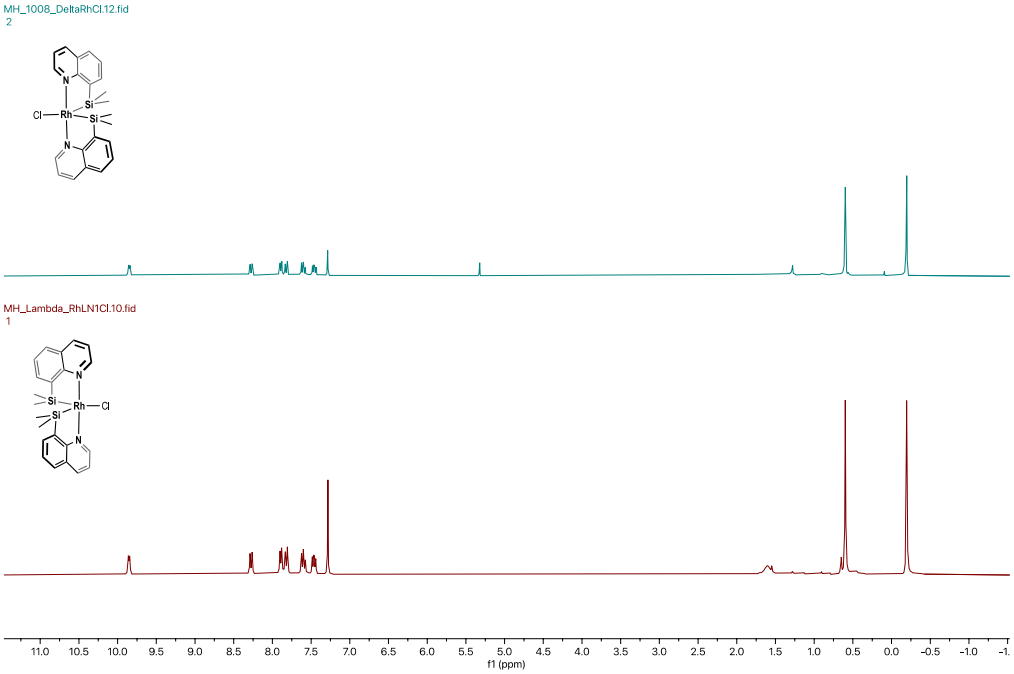

Figure S.12. ^{1}H NMR ($CDCl_3$) comparison between **Δ-Rh(SiN)$_2$Cl** (top) and **Λ-Rh(SiN)$_2$Cl** (bottom).

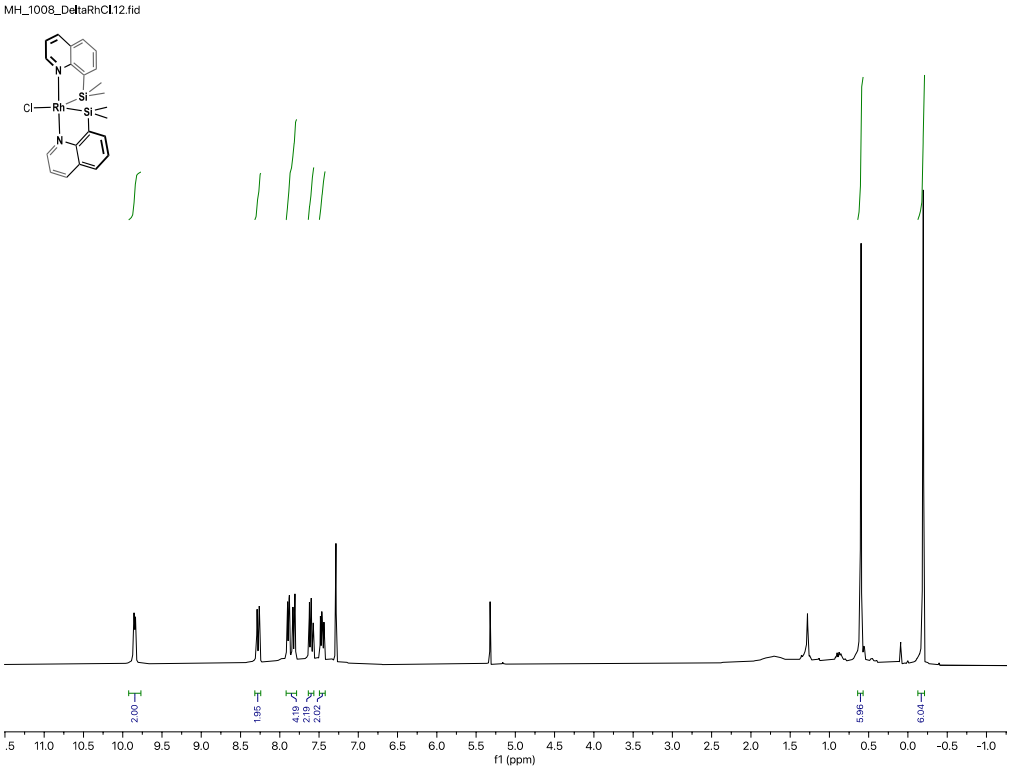

Figure S.13. ^{1}H NMR ($CDCl_3$) of **Δ-Rh(SiN)$_2$Cl.**

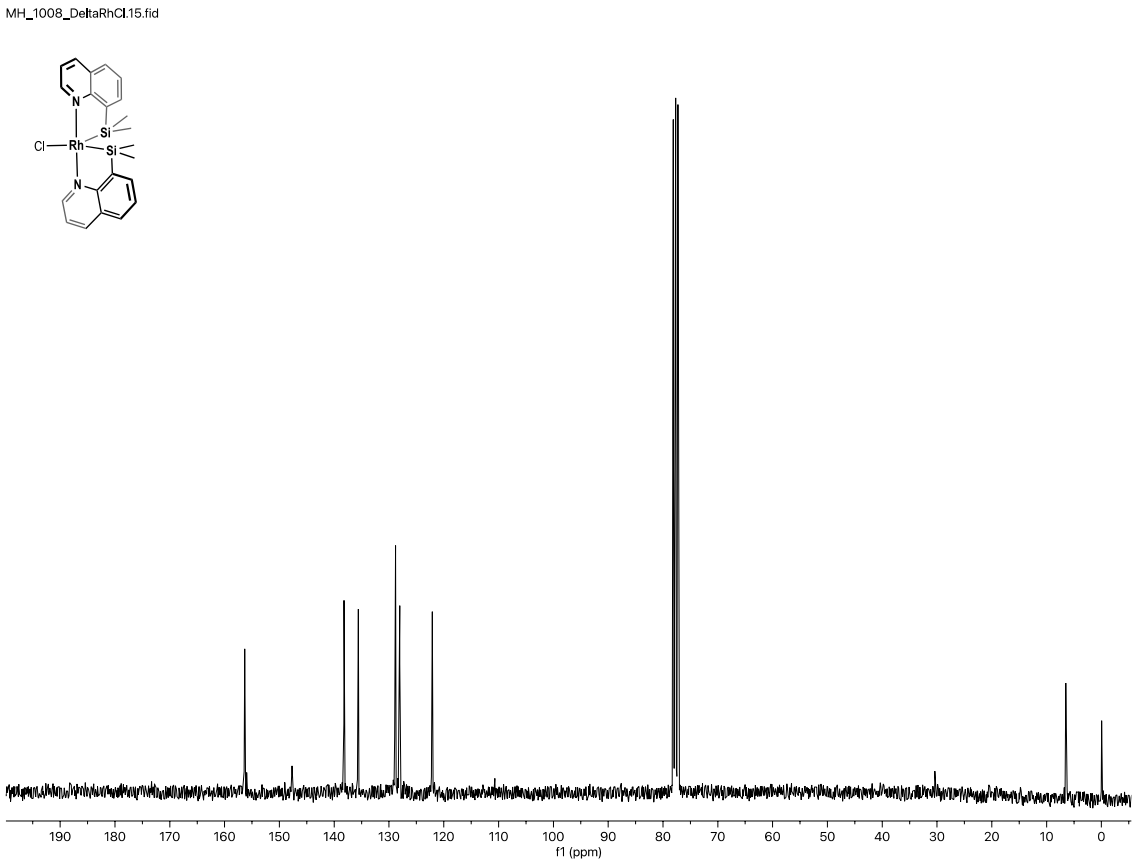

Figure S.14. $^{13}C\{^{1}H\}$ NMR ($CDCl_3$) of **Δ-Rh(SiN)$_2$Cl.**

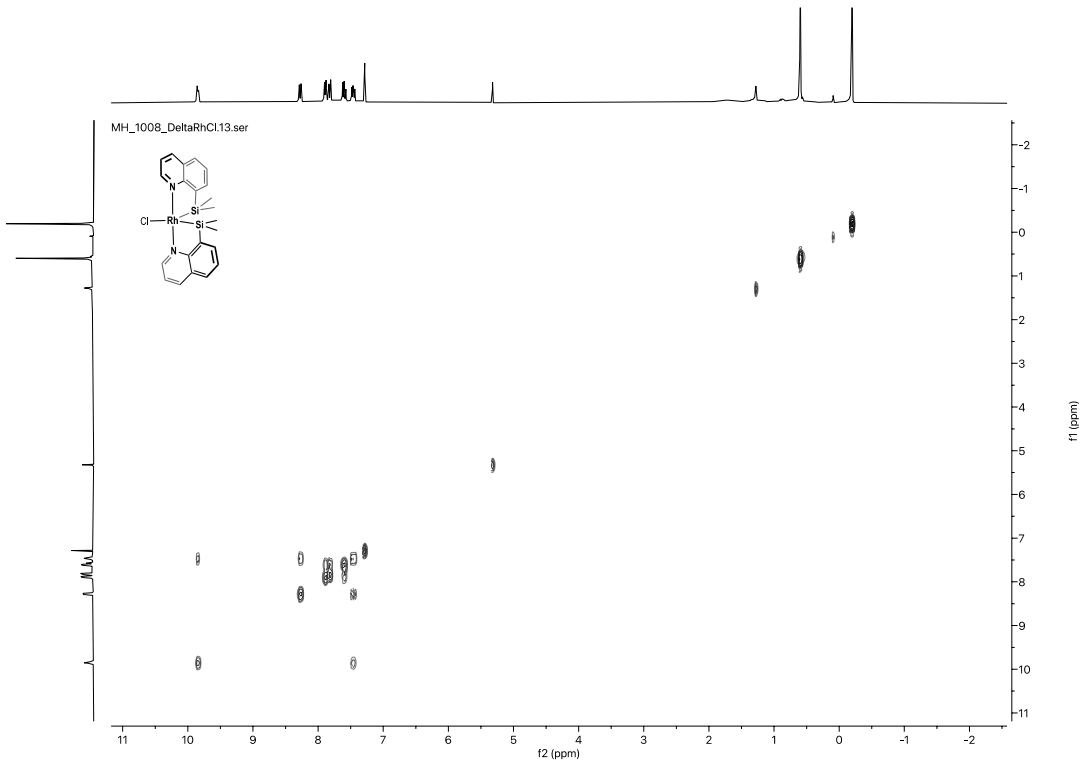

Figure S.15. $^{1}H/^{1}H$ COSY NMR ($CDCl_3$) of **Δ-Rh(SiN)$_2$Cl.**

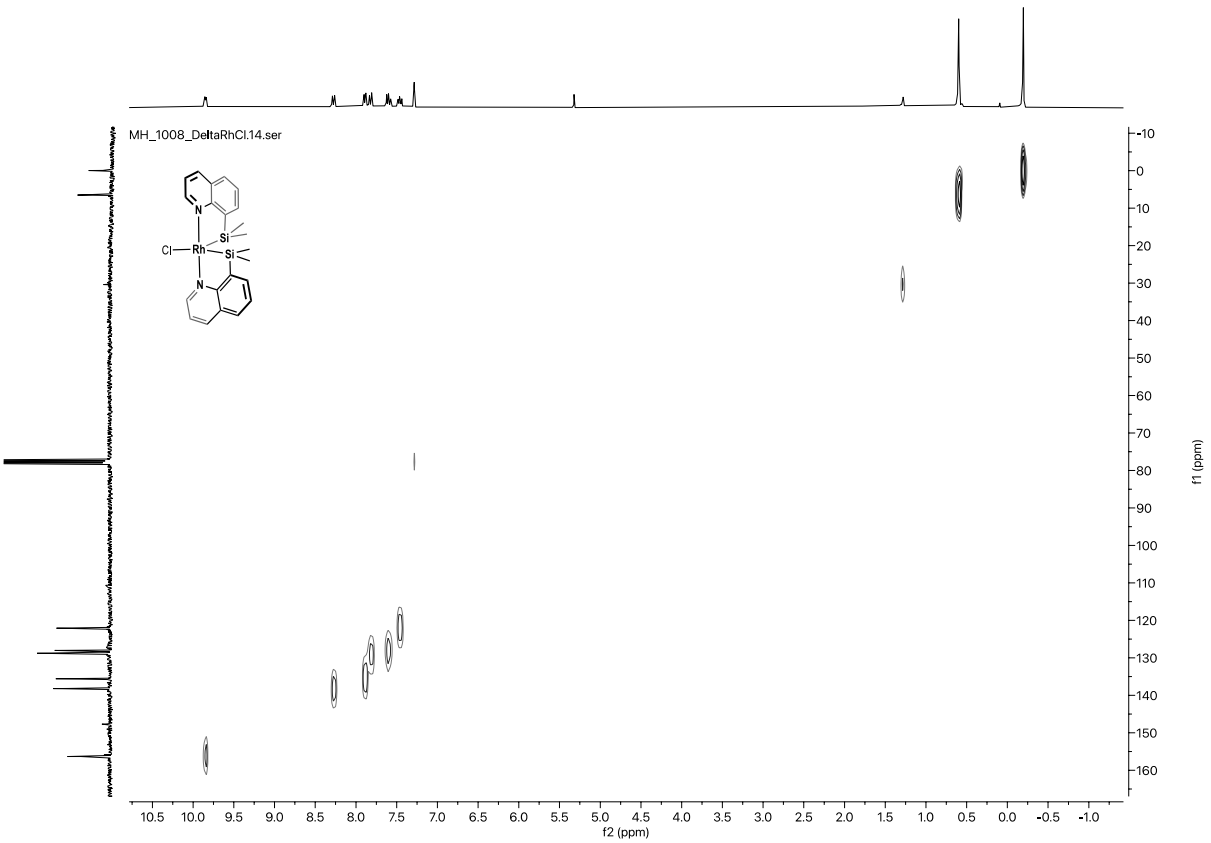

Figure S.16. $^{13}C/^{1}H$ HSQC NMR ($CDCl_3$) of **Δ-Rh(SiN)$_2$Cl.**

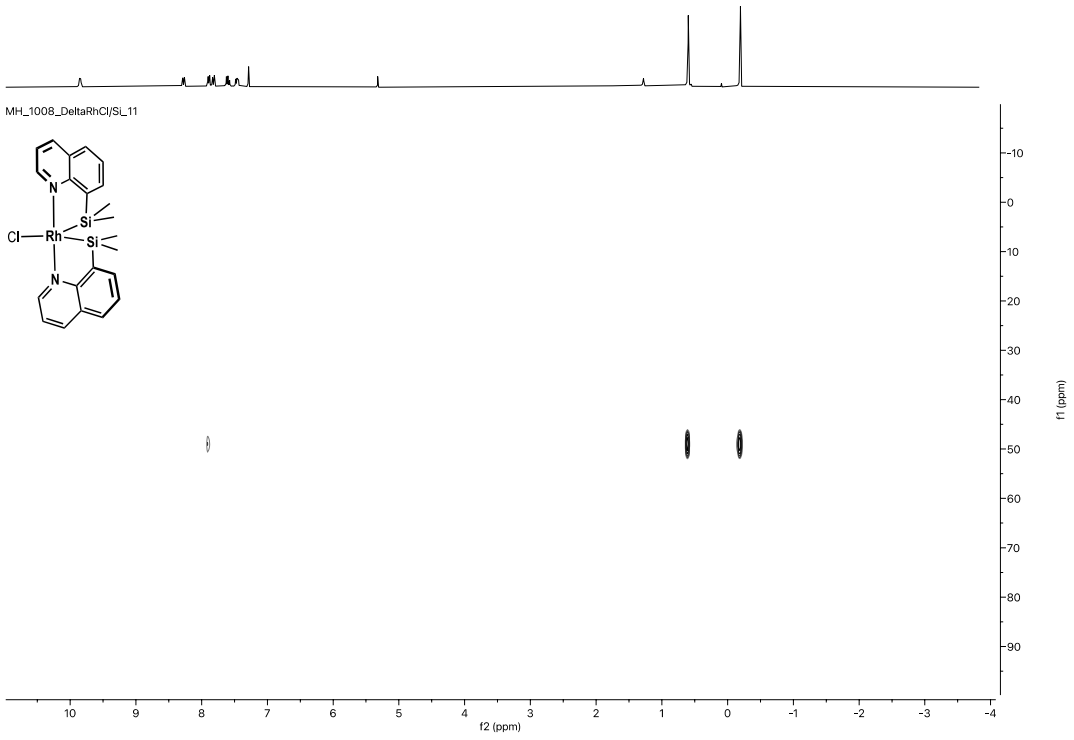

Figure S.17. $^{1}H/^{29}Si$ HMBC NMR ($CDCl_3$) of **Δ-Rh(SiN)$_2$Cl.**

4.3 Δ-Rh(SiN)$_2$[BAr$^F_4$] and Λ-Rh(SiN)$_2$[BAr$^F_4$]

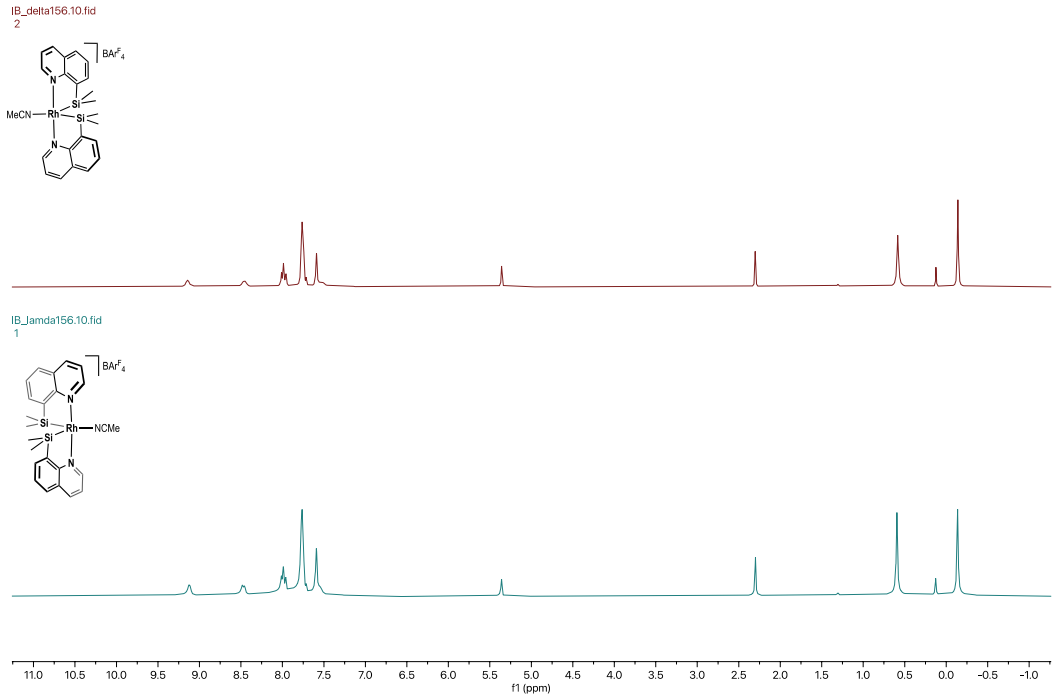

Figure S.18. ^{1}H NMR (CD_2Cl_2) comparison between **Δ-Rh(SiN)$_2$[BAr$^F_4$]** (top) and **Λ-Rh(SiN)$_2$[BAr$^F_4$]** (bottom).

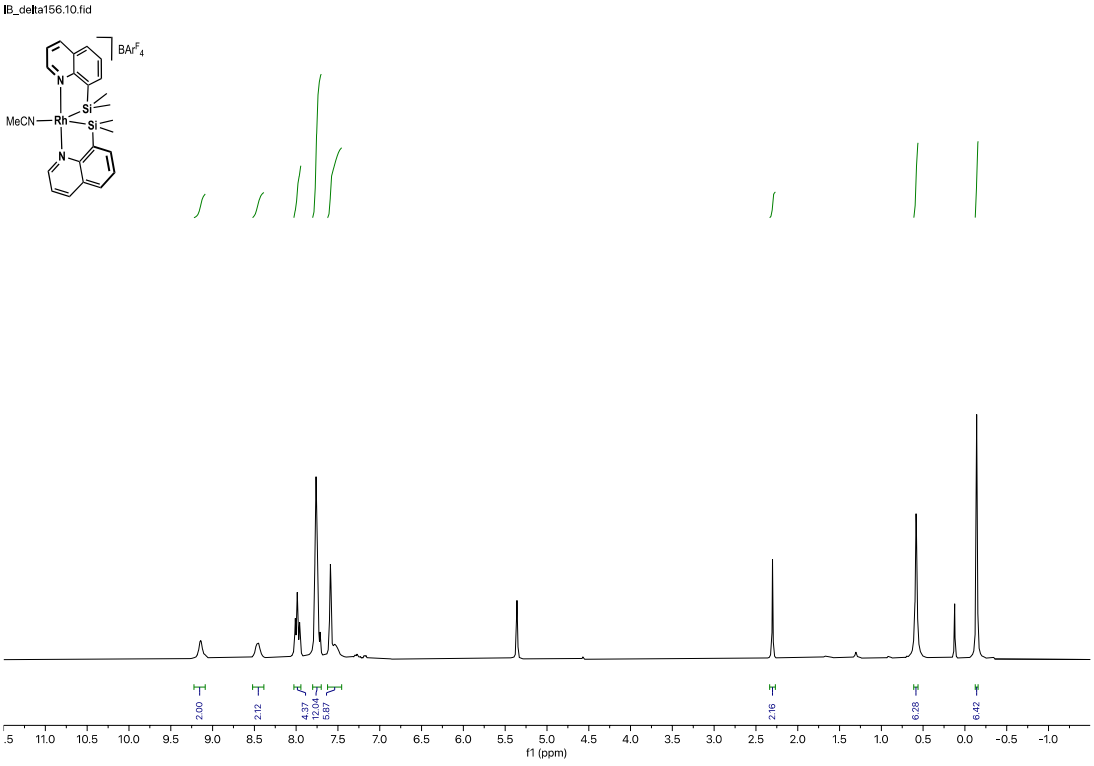

Figure S.19. ^{1}H NMR (CD_2Cl_2) of **Δ-Rh(SiN)$_2$[BAr$^F_4$]**.

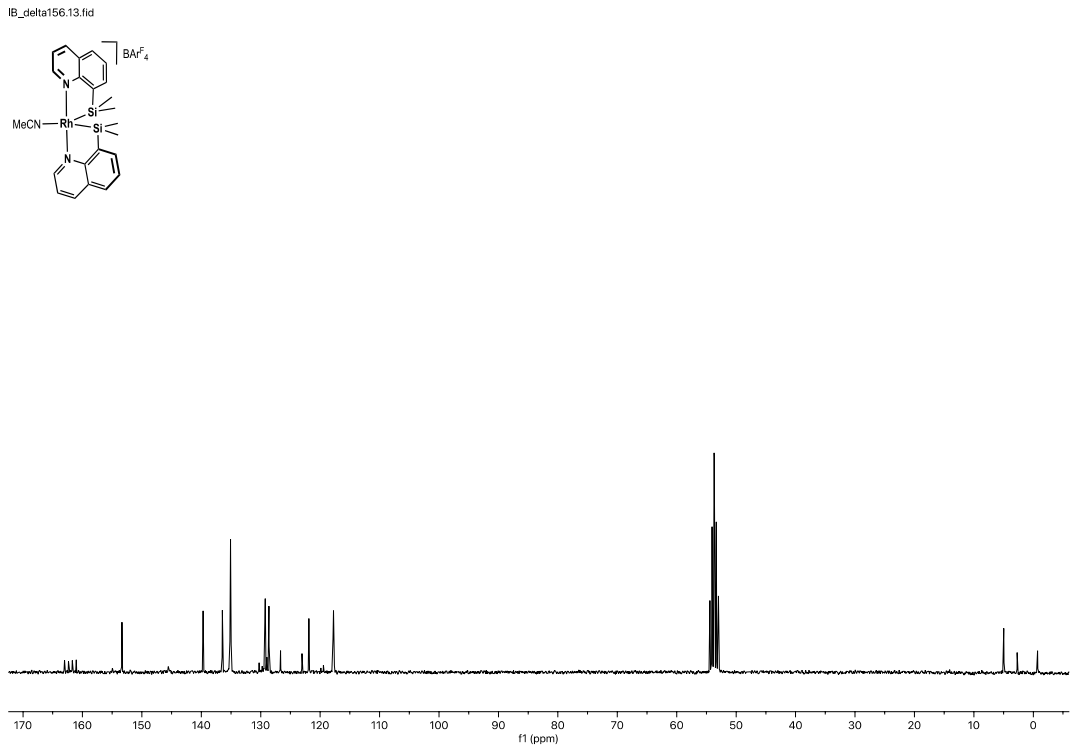

Figure S.20. $^{13}C\{^1H\}$ NMR (CD_2Cl_2) of **Δ-Rh(SiN)$_2$[BAr$^F_4$]**.

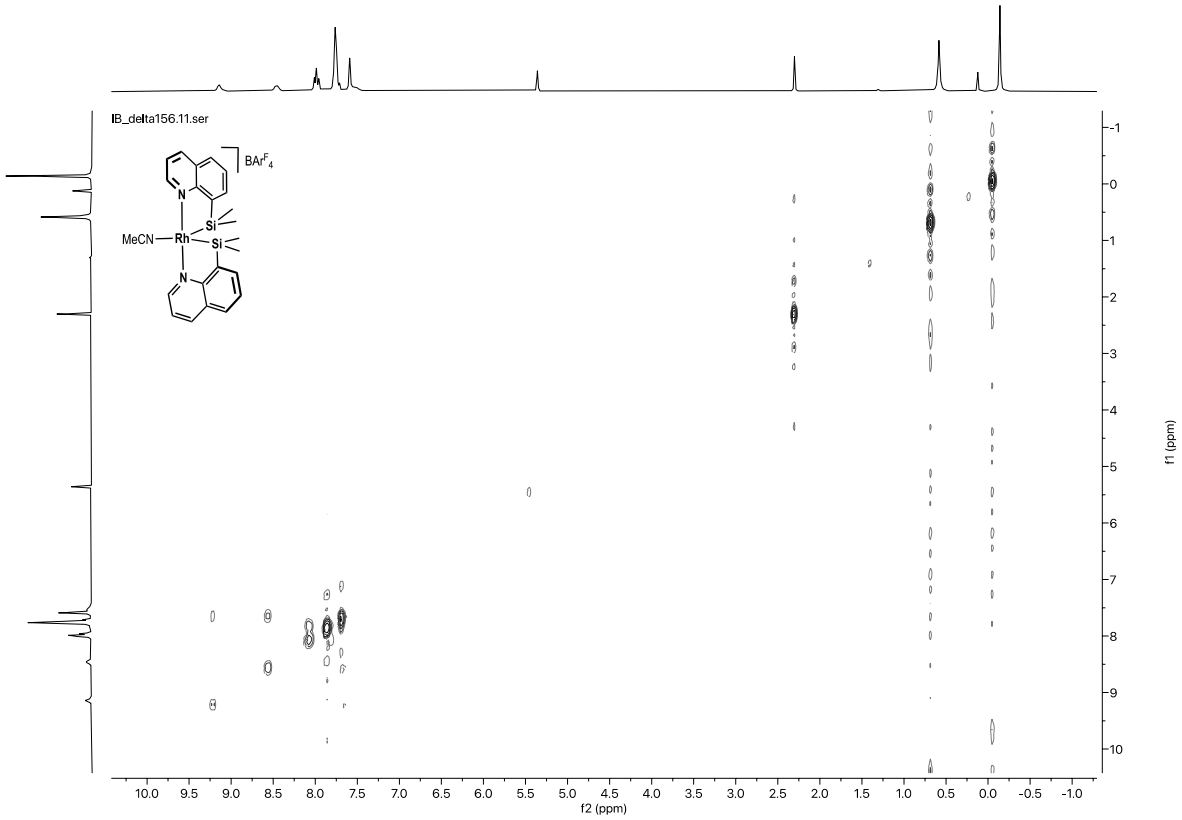

Figure S.21. $^1H/^1H$ COSY NMR (CD_2Cl_2) of **Δ-Rh(SiN)$_2$[BAr$^F_4$]**.

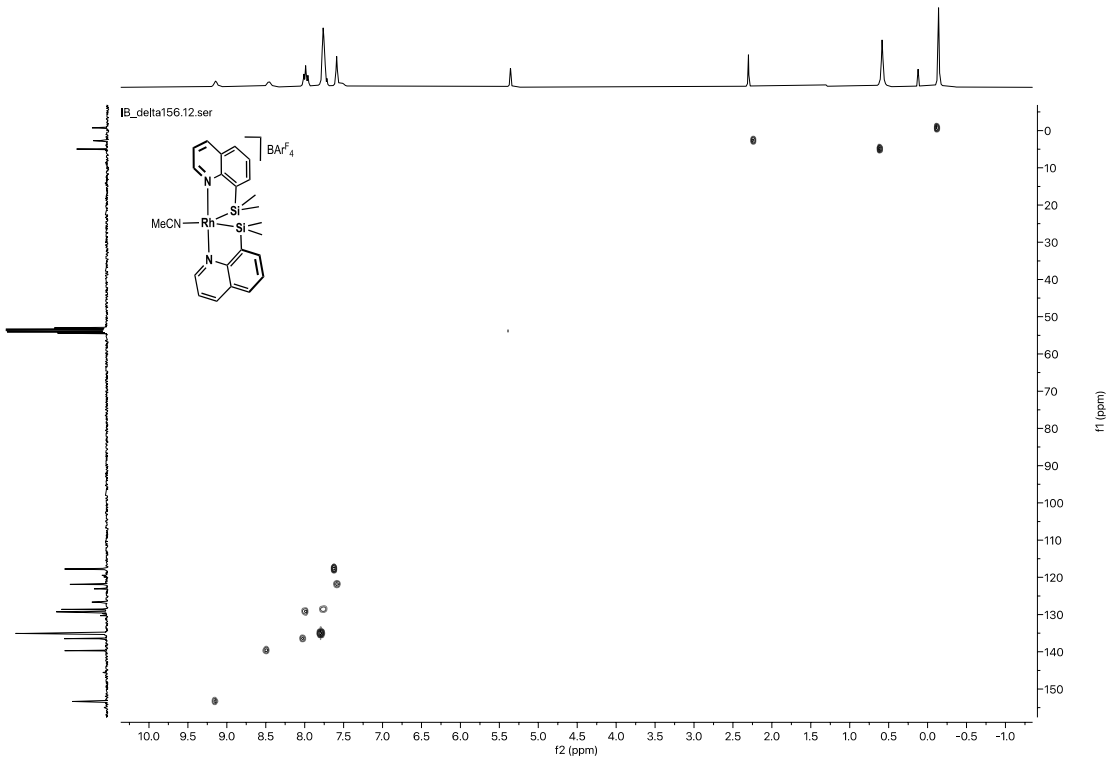

Figure S.22. $^{13}C/^{1}H$ HSQC NMR (CD_2Cl_2) of **Δ-Rh(SiN)$_2$[BAr$^F_4$].**

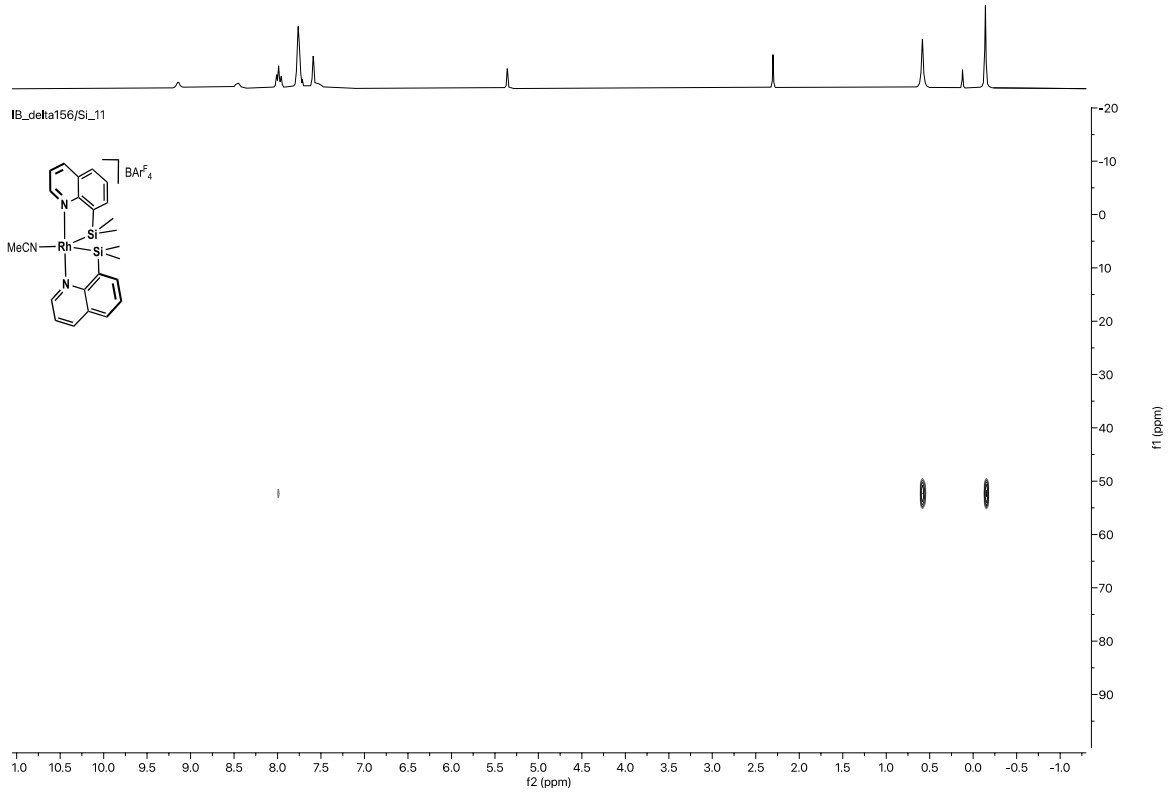

Figure S.23. $^{1}H/^{29}Si$ HMBC NMR (CD_2Cl_2) of **Δ-Rh(SiN)$_2$[BAr$^F_4$].**

5. ESI-MS

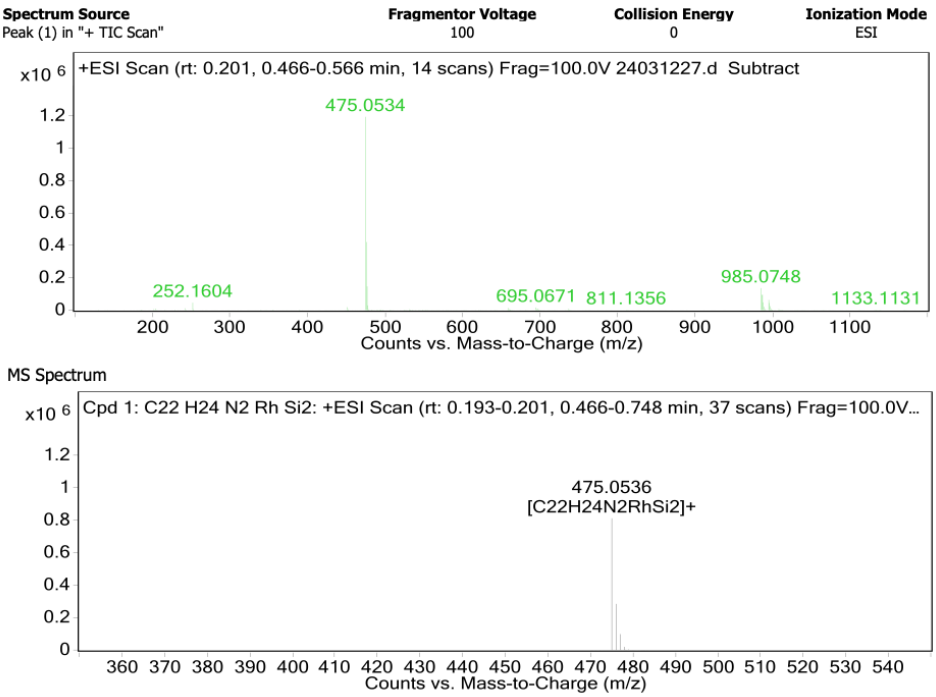

Figure S.24. ESI-MS of **Λ-Rh(SiN)$_2$(*R*-B(*S*-Man)$_2$)**

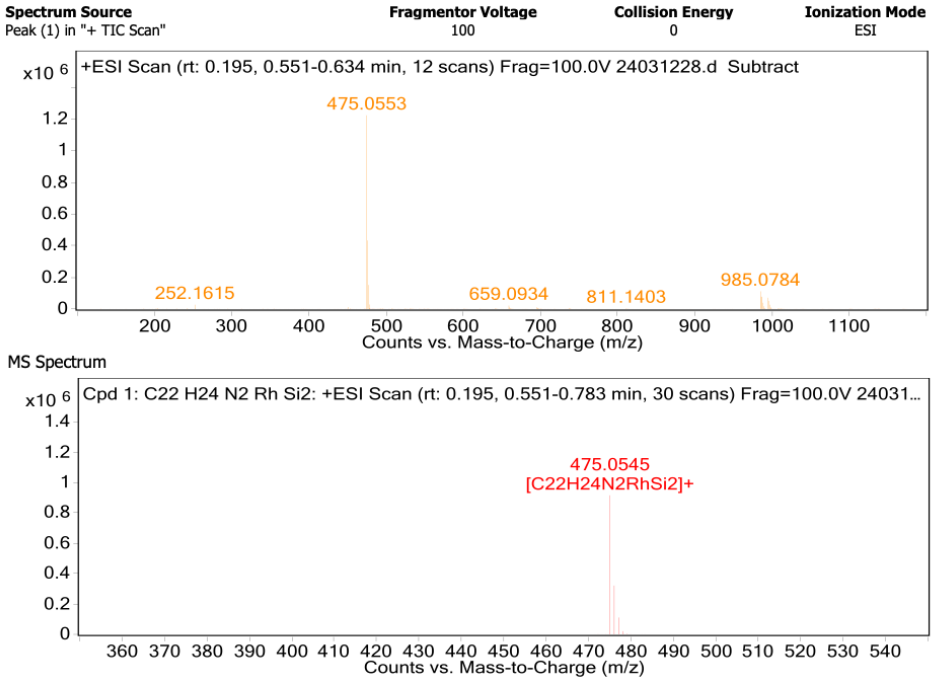

Figure S.25. ESI-MS of **Δ-Rh(SiN)$_2$Cl.**

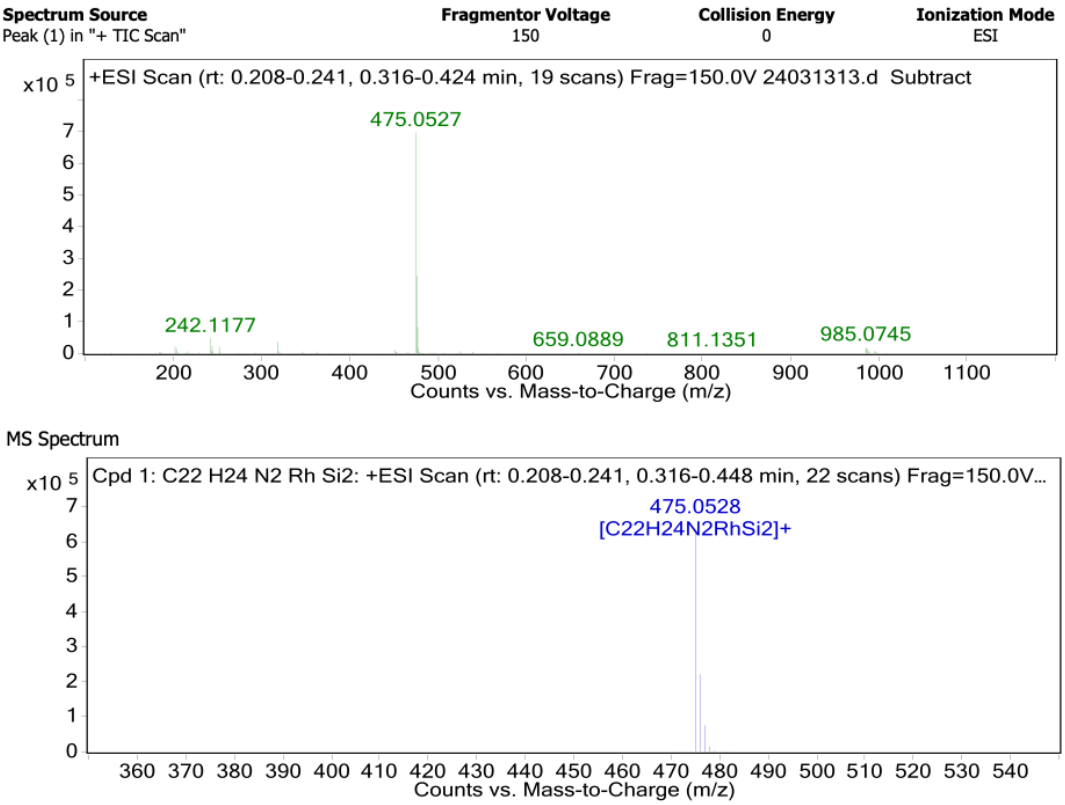

Figure S.26. ESI-MS of **Δ-Rh(SiN)$_2$[BAr$^F_4$]**.

6. X-Ray

Single crystal X-ray diffraction studies were performed on a Bruker D8-venture diffractometer equipped with a Mo Kα X-ray source (λ = 0.71073 Å) and a Photon3 detector. The temperature during data collection was controlled by means of a dry N_2 cryostream (Oxford Cryostream 700). Suitable single crystals were selected and mounted on MiTeGen polymer loops. APEX 3 software was used to collect and reduce the data. Adsorption corrections were applied using empirical methods using symmetry equivalent reflections combined with measurements at different azimuthal angles implemented using SADAPS. The structure was initially solved using the SHELXT[6] program using an intrinsic phasing method implemented through OLEX2 (v1.5),[7] and refined using SHELXL[8] least squares refinement procedures against all F^2 values. All non-hydrogen atoms were refined anisotropically. Hydrogen atoms were placed in calculated positions and refined with idealized geometries and assigned fixed occupancies and isotropic displacement parameters. Data for compound **Δ-Rh(SiN)$_2$(*R*-B(*S*-Man)$_2$)** was found to be twinned and thus processed as two-component twin. Final R(F), wR(F2) and goodness of fit agreement factors, details on the data collection and analysis can be found in Table S1. CCDC 2341547 and 2341546 contain the supplementary crystallographic data for compounds **Λ-Rh(SiN)$_2$(*S*-B(*R*-Man)$_2$)** and **Δ-Rh(SiN)$_2$(*R*-B(*S*-Man)$_2$)**, respectively. These data can be obtained free of charge from The Cambridge Crystallographic Data Centre via www.ccdc.cam.ac.uk/data_request/cif

	Λ-Rh(SiN)$_2$(*S*-B(*R*-Man)$_2$)	**Δ-Rh(SiN)$_2$(*R*-B(*S*-Man)$_2$)**
CCDC number	2341547	2341546
Formula	$C_{38}H_{36}N_2O_6Si_2Rh$	$C_{38}H_{36}N_2O_6Si_2Rh{\cdot}CH_2Cl_2$
M	786.59	871.51
Crystal System	monoclinic	orthorhombic
Space group	P21	P212121
T [K]	150	150
a [Å]	10.2080(8)	8.5875(7)
b [Å]	8.5609(7)	22.565(2)
c [Å]	21.3464(16)	40.397(3)
α [deg]	90	90
β [deg]	101.940(2)	90
γ [deg]	90	90
V [Å^3]	1825.1(2)	7828.0(12)
Z	2	8
Density [gcm^{-3}]	1.431	1.479
μ [mm^{-1}]	0.582	0.683
Reflections collected	37157	16076
R_1 [I > 2σ(I)]	0.0587	0.0658
wR_2 [all data]	0.1606	0.1667
GoF	1.101	1.025
Flack parameter	0.02(3)	0.06(3)

[a] $\sum||F_o|-|F_c||/\sum|F_o|$ [b] $\{\sum [w(F_o^2-F_c^2)^2]/\sum [w(F_o^2)^2]\}^{1/2}$

Table S1. Crystallographic data and structure refinement details of all compounds.

7. ECD

CD spectra were recorded on a Jasco J-1500 spectropolarimeter. The concentration of all samples was 3 x 10^{-5} M in CH_2Cl_2.

Model	J-1500
Detector	PM-539
Light Source	Xenon
CD Overload detect	216
Measure range	450-220 nm
T [K]	298
Data pitch	1 nm
CD scale	200 mdeg/0.1dOD
D.I.T.	1 sec
Bandwidth	10 nm
Scanning mode	continuous
Scanning speed	500 nm/min
Reflections collected	37157
No. of cycle	1

8. Catalysis

Rhodium-catalyzed hetero Diels-Alder reaction.

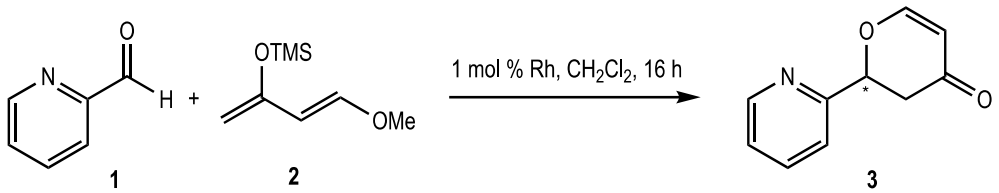

Procedure: A Young's Schlenk was filled with rhodium catalyst (1 mol%) and pyridine-2-carbaldehyde (**1**, 19 μL, 0.2 mmol) and placed under argon. 2 mL of dry dichloromethane was added via syringe. After 30 minutes trans-3-(tert-butyldimethylsiloxy)-1-methoxy-1,3-butadiene (**2**, 95 μL, 0.4 mmol) was added and reacted under argon for 24 hours. After that time a ^{1}H NMR of the reaction crude was performed to obtain the conversion (aldehyde remaining). The reaction crude was extracted with water, the dichloromethane was dried with $MgSO_4$ and the solvent was evaporated. The product obtained was purified by chromatography with silica gel (Hexane/AcOt= 1:1) obtaining **3**: 30 mg (*rac*-**Rh(SiN)$_2$[BAr$^F_4$]**), 31 mg (Λ-**Rh(SiN)$_2$[BAr$^F_4$]**), 28 mg (Δ-**Rh(SiN)$_2$[BAr$^F_4$]**). The enantiomeric ratios were calculated by HPLC chromatography with a chiral column.

Characterization of 5: ^{1}H NMR ($CDCl_3$) δ 8.64 (d, J = 5.1 Hz, 1H), 7.80 (td, J= 7.7, 2.2 Hz, 1H), 7.52 (m, 1H), 7.50 (m, 1H), 7.33 (dd, J= 7.7, 5.1 Hz, 1H), 5.59 (m, 1H), 5.56 (m, 3H), 2.97 (m, 2H).

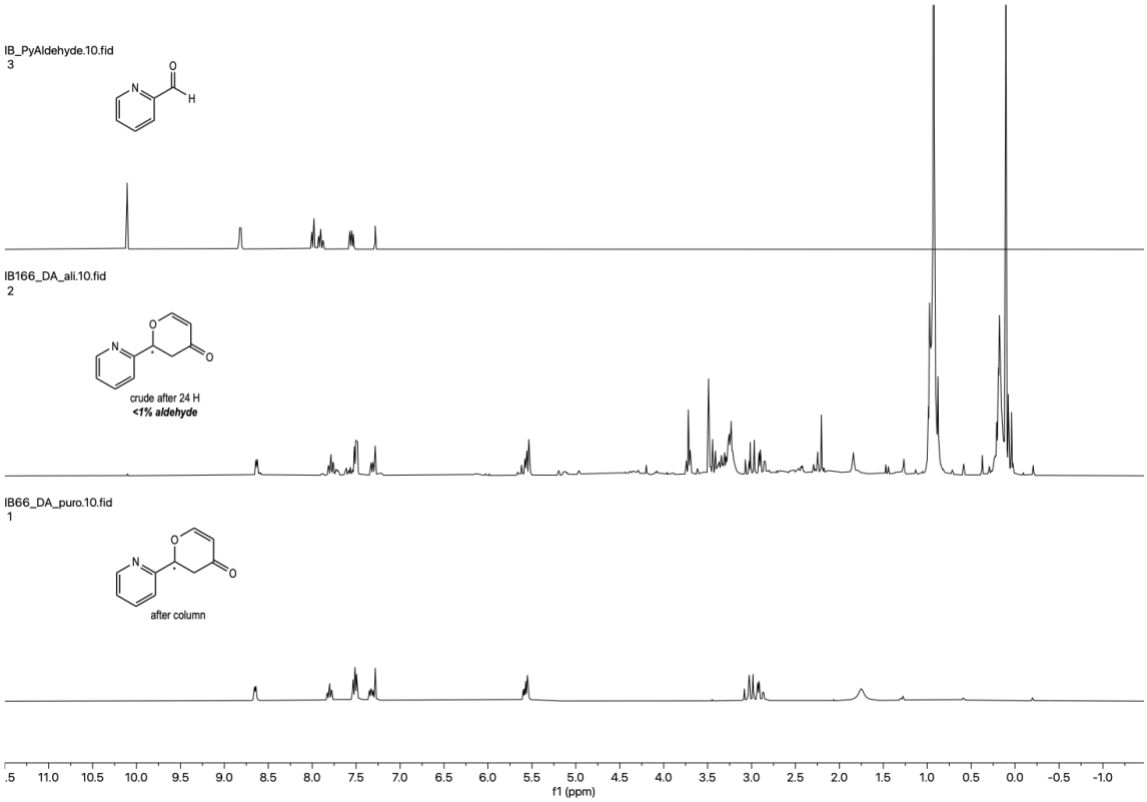

Figure S.27. ^{1}H NMR ($CDCl_3$) of: pyridine-2-carbaldehyde (top), reaction crude (middle) and **5** (bottom).

HPLC: AD-H, Hex/IPrOH= 90:10, Flow rate= 0.5 mL·min^{-1}, 25 ºC

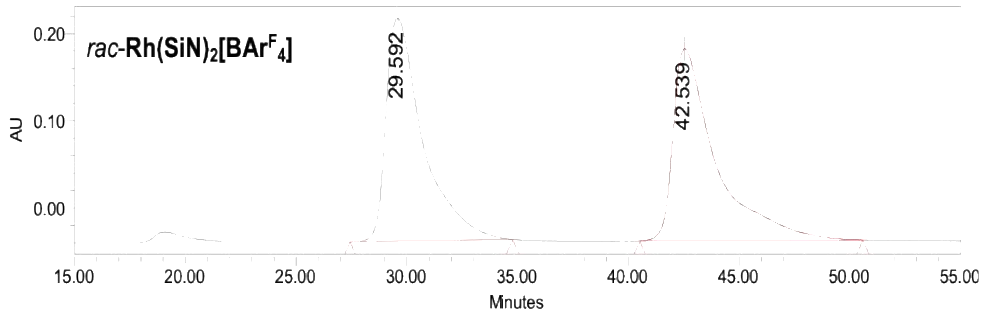

	Retention Time	% Area
1	29.592	49.80
2	42.539	50.20

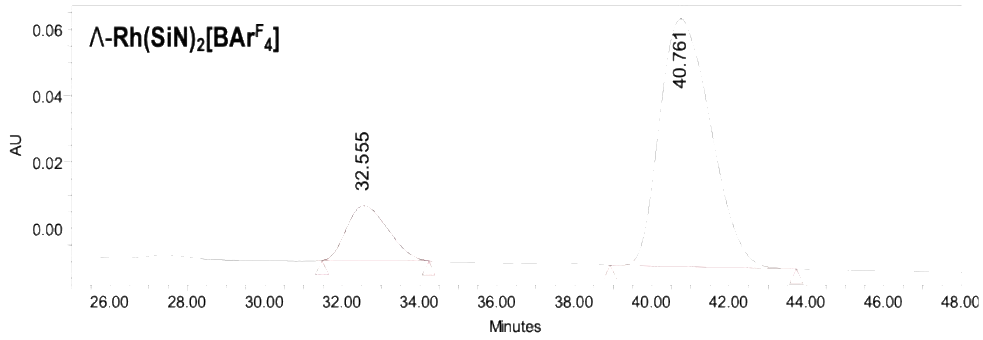

	Retention Time	% Area
1	32.555	15.23
2	70.761	84.77

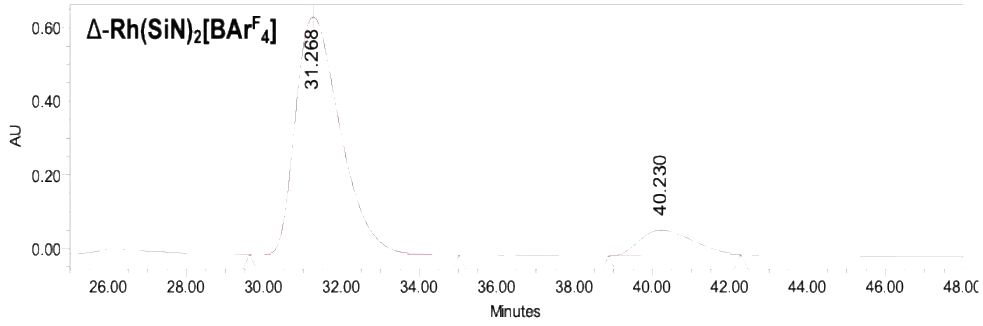

	Retention Time	% Area
1	31.286	88.88
2	40.230	11.12

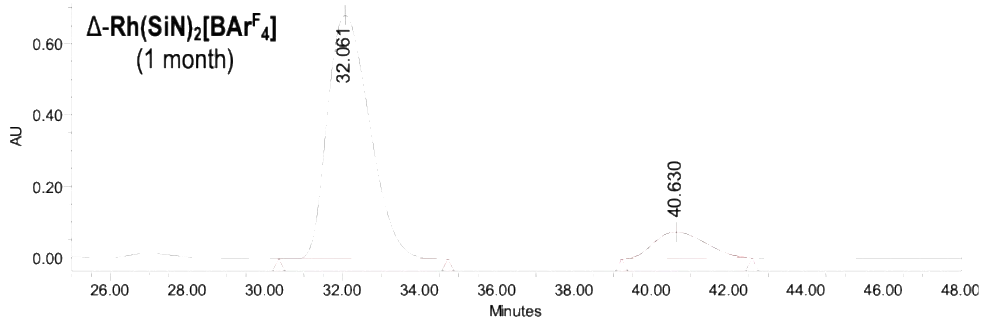

	Retention Time	% Area
1	32.061	88.23
2	40.630	11.77

Figure S.28. HPLC spectra and tables with retention times and integrated areas.

9. References

(1) U. Prieto-Pascual, I. V. Alli, I. Bustos, I. J. Vitorica-Yrezabal, J. M. Matxain, Z. Freixa, and M. A. Huertos, *Organometallics*, 2023, **42**, 2991-2998.

(2) U. Prieto-Pascual. A. Martinez de Morentin, D. Choquesquillo Lazarte, A. Rodriguez-Dieguez, Z. Freixa, and M. A. Huertos, *Dalton Trans*., 2023, **52**, 9090-9096

(3) L. W-Y. Wong, J. W-H. Kan, T. Nguyen, H. H-Y. Sung, D. Li, A. S-F. Au-Yeng, R. Sharma, Z. Lin, and I. D. Williams, *Chem. Commun.* 2015, **51**, 15760-15763.

(4) M. Brookhart, B. Grant, and A. F. Volpe Jr., *Organometallics* 1992, **11**, 3920.

(5) L. Falivene, Z. Cao, A. Petta, L. Serra, A. Poater, R. Oliva, V. Scarano and L. Cavallo, *Nat. Chem*. 2019, **11**, 872-879.

(6) G. M. Sheldrick, *Acta Cryst. A*, 2015, **71**, 3-8.

(7) O. V. Dolomanov, L. J. Bourhis, R. J. Gildea, J. A. K. Howard and H. Puschmann, *J. Appl. Cryst.,* 2009, **42**, 339-341

(8) G. M. Sheldrick, *Acta Cryst. C*, 2015, **71**, 3-8.